# Electron-beam induced degradation in CdTe photovoltaics

R. Harju, V. G. Karpov,[a] D. Grecu, and G. Dorer
*First Solar LLC, 12900 Eckel Junction Road, Perrysburg, Ohio 43551*

(Received 9 March 2000; accepted for publication 15 May 2000)

We used electron beam induced current (EBIC) to measure degradation of CdTe photovoltaic cells. We have observed that: (i) the EBIC signal shows a considerable, continuous degradation depending on the electron-beam current, scan area, energy, and sample treatment; (ii) the characteristic degradation time fluctuates between different spots on the same sample; and (iii) grain boundary regions are the most effective collectors of the electron-beam generated charge carriers. Our phenomenological model relates the observed degradation to defects caused by the electron-beam generated electrons and holes. © *2000 American Institute of Physics.* [S0021-8979(00)04416-9]

## I. INTRODUCTION

In order to become competitive and gain market share, it was estimated that thin-film photovoltaic (PV) modules must be guaranteed a lifetime of approximately 20 yr.[1] Much interest has been expressed recently towards the design of accelerated lifetime testing procedures to allow the prediction of module stability in a relatively short period. Light-induced effects accumulate slowly and sometimes become significant only after several years. In addition, factors such as temperature and ambient variations are not well controlled in this time frame and thus obscure the observations. Consequently, conducting accelerated life tests requires techniques able to produce effects similar to those induced by light on a much shorter time scale and under well-controlled conditions.

Electron-beam irradiation is a potential candidate that may satisfy the above criteria. Electron beams with a diameter of approximately 100 A, energies of 10–30 keV, and currents 0.01–10 nA are typically available in electron microscopes. They do not produce much heating and are not energetic enough to cause atomic displacements which in this respect are equivalent to light.[2] However, in semiconductor materials, electron beams can lead to electron–hole pair generation rates up to $10^5$ higher than light (AM1.5). One additional advantage of the technique is that the degradation can be measured continuously *in situ* by monitoring the electron beam induced current (EBIC).

Most of the previous work on electron-beam induced degradation has been devoted to *a*-Si:H, although similar effects were found in a variety of other semiconductors.[2] In *a*-Si:H, *e* beams generate metastable defects comparable to those caused by illumination, although certain differences exist in the kinetics of the two processes.[2] In this article, we investigate the degradation of CdTe PV devices induced by electron-beam excitation. As in the case of *a*-Si devices, we suggest that the degradation mechanisms are similar to those produced by light illumination. In addition, we propose a theoretical model for the observed degradation that is consistent with our data.

[a]Author to whom correspondence should be addressed; electronic mail: vkarpov@firstsolar.com

## II. EXPERIMENT

The typical experimental device in this study consists of a 0.3 $\mu$m layer of CdS followed by a 3.5–4 $\mu$m CdTe layer deposited on commercially available $SnO_2$-coated glass substrates.[3] The conductive oxide layer has a sheet resistance of 12 $\Omega$ and serves as the front electrode. The semiconductor layers were deposited using a proprietary vapor transport deposition method. After deposition, the samples were submitted to a standard anneal in the presence of $CdCl_2$ vapors, which generally leads to improved electrical characteristics.[4] After this anneal, typical grain sizes for CdTe are 1–2 $\mu$m. A metal layer deposited by sputtering was used to form the back contact to CdTe. Cu was introduced at the metal–semiconductor junction through an anneal step.[1] This step is believed to lead to the formation of a strongly doped *p* layer at the surface of the CdTe and help in the formation of a good back contact.[5] The use of Cu in this study was motivated by results of recent studies suggesting that Cu electromigration and instability in the CdTe matrix could lead to significant device degradation.[6,7]

The EBIC analysis was carried out in a JEOL JSM T-330 electron microscope using back-wall excitation geometry, with injection through the back contact and CdTe. The digital output was read with a digital multimeter having a PC interface. We used electron energies varying from 10 to 30 keV and beam currents $I_e$ varying from 0.5 to 3 nA.

The electron beam generates electron–hole ($e-h$) pairs in a localized teardrop-shaped region whose position and size inside the device depend on the electron energy $W$.[8] The distance from the back contact to the center of the generation region varies monotonically with the electron energy from 2.6 $\mu$m at 20 keV to 5.1 $\mu$m at 30 keV. The characteristic spatial dispersion of excited $e-h$ pairs is approximately three times smaller than the above distance. The beam scans an area of a given size (ranging from 0.5 to 13 200 $\mu m^2$ in our experiments, much larger than the beam cross section) and the generation region follows the beam adiabatically. (Relaxation times in the electron and phonon systems of the material are much shorter than the characteristic time it takes the beam to travel the generation region length.) The built-in electric field at the $p-n$ junction spatially separates the elec-

 

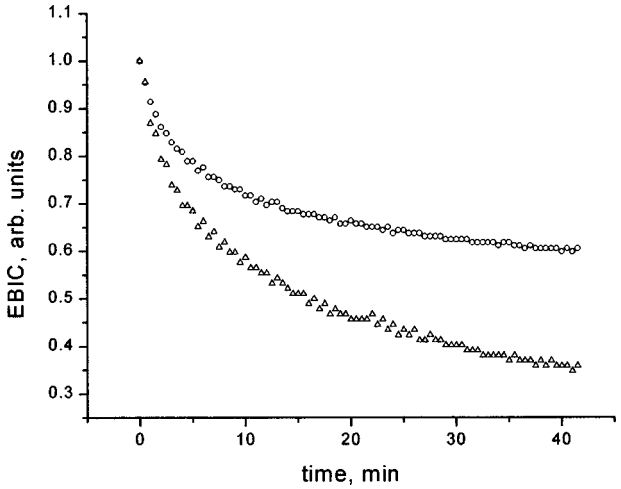


FIG. 1. Normalized EBIC degradation at two different spots of the same sample. *e*-beam parameters: $I_e=0.8$ nA, $E=20$ keV, $A=530\ \mu\text{m}^2$.

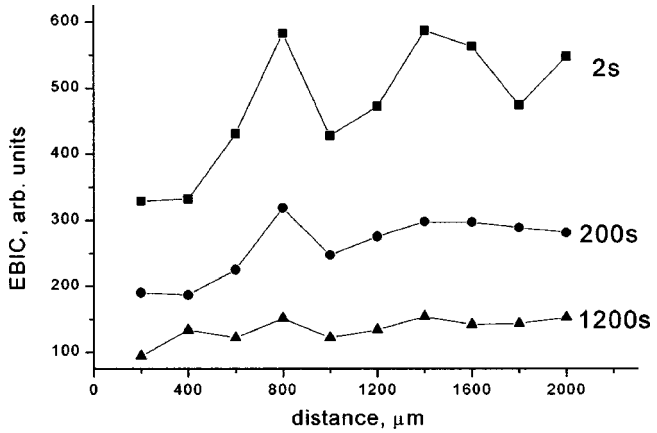


FIG. 2. EBIC degradation vs spot location in the same sample at different times. *e*-beam parameters: $I_e=0.58$ nA, $E=20$ keV, $A=530\ \mu\text{m}^2$.

trons and holes pulling them to the opposite electrodes, thus generating the EBIC $J$. In our experiments we measured $J$ as a function of scan time $t_s$, scan area $A$, electron energy $E$, and beam current $I_e$.

The beam generates $e-h$ pairs at an extremely high rate. For example, for a beam of diameter $d$ 0.5 $\mu$m, current $I_e$ 1 nA, electron energy $W$ 30 keV, spatial dispersion length $l$ 1 $\mu$m, and $e-h$ pair generation energy $w$ 5 eV (triple the band gap),[8] the effective $e-h$ generation rate is

$$g_e=\frac{I_e}{d^2 le}\left(\frac{W}{w}\right)\approx 10^{26}\ \text{cm}^{-3}\,\text{s}^{-1}. \tag{1}$$

Here $e$ is the electron charge; the role of backscattered electrons is not included. This equation yields the acceleration factor of $a=g_e/g_l\approx 10^5$ as compared to the standard light-generation rate, $g_l\approx 10^{21}\,\text{cm}^{-3}\,\text{s}^{-1}$. As is shown below [see the discussion after Eqs. (6) and (10)], the material degradation rate can be either linear or nonlinear in the excitation intensity $g_e$.

Note that the $e-h$ generation rate does not change with the scan area $A$, since physical generation occurs locally under the beam. Instead, the time that the beam spends on a given local spot in the scanned area decreases with $A$. Assuming the generation region area $\sigma \ll A$, the local irradiation (true) time

$$t=\frac{\sigma}{A}t_s \ll t_s, \tag{2}$$

where $t_s$ is the measured scanning time. Because decrease in irradiation time is not generally equivalent to decrease in generation rate, the difference between light-induced and *e*-beam induced degradations does not necessarily reduce to the above acceleration factor.

Figure 1 shows a typical observed EBIC degradation; more data are presented below in comparison with the theoretical fit (Figs. 7 and 8). The EBIC signal shows a considerable variability between different spots on the same sample. The variability decreases with the irradiation dose. Figure 2 illustrates the case of ten equidistant spots along a straight line in one of the examined samples. Note that similar spatial variations were observed earlier in the laser beam induced current in CdTe solar cells[9] and were found to increase with the generation intensity.

To study the reversibility of the *e* beam induced degradation we used a time-modulated *e* beam. When the beam is turned off the current drops a certain value with any transient effects appearing to have time constants less than 1 min. As can be observed in Fig. 3, the EBIC degradation is partly reversible. Figure 4 illustrates changes in the EBIC signal during 15 h interruption in continuous irradiation showing the same partial reversibility trend.

Figure 5 shows changes in the EBIC signal when the scanned area $A$ is successively increased every 15 min of irradiation, starting from 5 $\mu\text{m}^2$ and going up to 13 200 $\mu\text{m}^2$. The fact that the EBIC signal depends on $A$ suggests that the irradiated material degrades and is consistent with the EBIC decay in time presented in Fig. 1. (For discussion, see Sec. III C.)

One side result of our EBIC studies is worth mentioning in connection with the observed degradation. We compared the secondary electron image to the EBIC image and found grain-boundary regions to be more effective current collec-

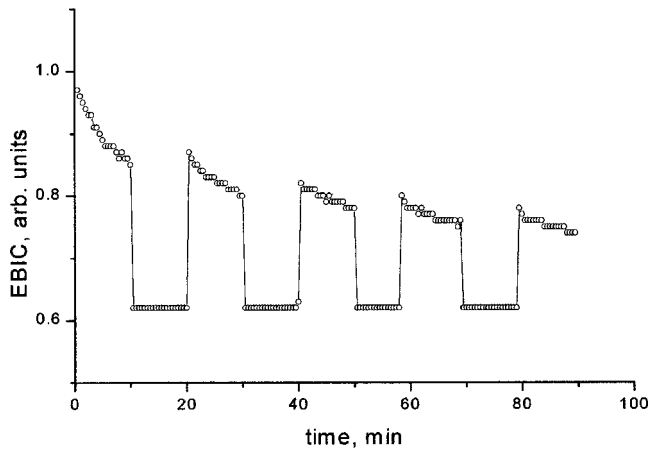


FIG. 3. EBIC degradation under modulated *e* beam. *e*-beam parameters: $I_e=0.8$ nA, $E=20$ keV, $A=30\ \mu\text{m}^2$.

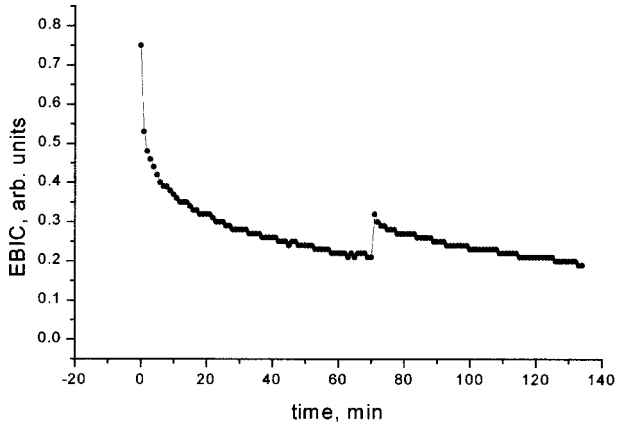


FIG. 4. Interrupted EBIC degradation: 15 h out of the beam after 70 min irradiation. *e*-beam parameters: $I_e=1.30$ nA, $E=25$ keV, $A=530\ \mu\text{m}^2$.

tors than the intragrain material (Fig. 6). The two images when superimposed produce a uniform black appearance. They are complimentary to each other as a negative to the photographic image. The ratio of the grain boundary to intragrain EBIC intensity can be as large as 100 (different etches changed the EBIC image and the ratio of intragrain to grain-boundary EBIC intensities.). Galloway *et al.*[10] reported a similar effect for CdTe cells.

We explain the increased collection at the grain boundaries by the presence of built-in electric fields that effectively separate nonequilibrium electron and holes and thus suppress their recombination. We note that the parameters of such fields, the amplitude $E$ and the screening length $L$, depend on local impurity (defect) concentration and thus fluctuate between different grain boundary regions. The corresponding recombination barrier ($V_\gamma=EL$) fluctuations make the recombination parameter [$\gamma\propto\exp(-V_\gamma/kT)$, where $kT$ is the thermal energy] fluctuate exponentially between different grain boundary regions. This nonuniformity may be the cause for the observed variations in degradation kinetics between different spots on the same sample, as we will discuss in more detail in Sec. III. Note that our EBIC topography diagrams show fluctuations in the current collections between different bright grain boundary regions.

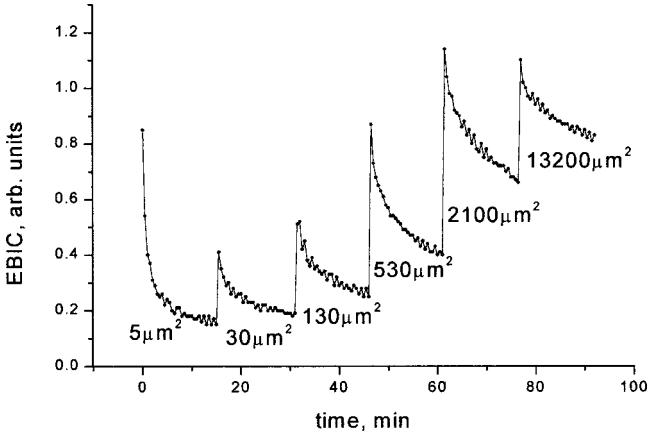


FIG. 5. Area dependent EBIC degradation with 15 min exposure at specified scan areas. *e*-beam parameters: $I_e=0.8$ nA, $E=20$ keV.

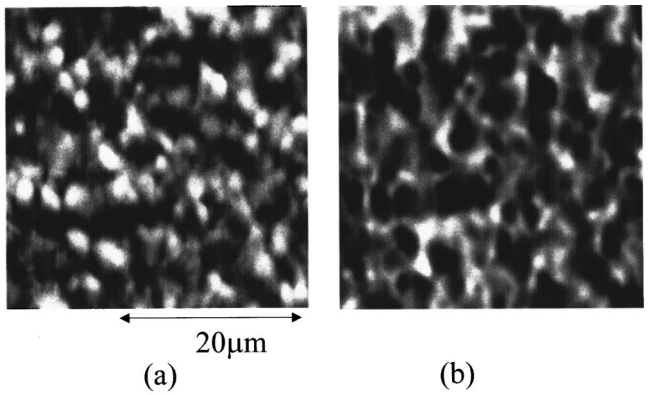


FIG. 6. EBIC image (a) in comparison with the secondary electron image (b). Bright spots in the EBIC map correspond to the grain boundary regions where EBIC is a maximum. *e*-beam parameters: $I_e=1.30$ nA, $E=25$ keV, $A=530\ \mu\text{m}^2$.

## III. MODEL

Our model relates the above-described phenomena to changes in the semiconductor absorber layer. We assume that the observed decay of the EBIC signal reflects changes in the charged-carrier concentration caused by *e*-beam induced defects. Our phenomenological model does not specify the microscopic nature of the defects, such as their chemical composition and lattice relaxation. It describes the simplest conceivable kinetics of material degradation in response to extra charge carriers.

We postulate that in the materials under consideration new defects appear in response to extra carriers (electrons and/or holes). This postulate reflects the fact that the material degrades because of irradiation with photons and electrons that are not energetic enough to create lattice displacements and interact with the electron subsystem. The same mechanism of defect creation may be responsible for the phenomenon of self-compensation that makes it impossible (or very hard) to dope the materials under consideration.[11] Indeed, because there is no difference between the charge carriers brought into the system by radiation and doping, the latter will trigger defect creation as well.

To summarize, we assume that: (i) the defect creation rate depends on charge carrier concentration and (ii) these defects act as recombination centers and thus have a feedback effect on the charge carrier concentration. Consequently, the kinetics of the charge carriers and photogenerated defects are coupled and must be considered self-consistently.

### A. Linear kinetics

In the simplest approximation the defect generation rate $dN/dt$ is linear in the charge carrier concentration $n$

$$\frac{dN}{dt}=\alpha n-\beta N. \tag{3}$$

Here the last term represent the process of defect annihilation; $\alpha$ and $\beta$ are material parameters. Both the parameters are in general temperature dependent as they describe the processes of defect creation and annihilation; these tempera-

ture dependences are normally of the activation type. Also, if the defect centers contain doping impurity atoms (as was suggested for the self-compensation phenomena and photo-induced defects[7,8]), then $\alpha$ and $\beta$ are impurity dependent. Because the electron kinetics is relatively fast (as compared to that of the defects) we can write the corresponding balance equation in the quasistationary approximation

$$G-\gamma Nn=0, \tag{4}$$

where $G$ is the electron–hole generation rate (the number of $e-h$ pairs created per time per volume), and $\gamma$ is the recombination constant. We have chosen here the recombination rate to be linear in electron concentration, which is a typical case in semiconductors.

The solution to the above equations is

$$\begin{aligned} N&=N_\infty\sqrt{1-\left[1-\left(\frac{N_0}{N_\infty}\right)^2\right]\exp(-2\beta t)},\\ &\text{where}\quad N_\infty=\sqrt{\alpha G/\gamma\beta},\\ n&=\frac{G/\gamma N_\infty}{\sqrt{1-\left[1-\left(\frac{N_0}{N_\infty}\right)^2\right]\exp(-2\beta t)}}. \end{aligned} \tag{5}$$

Here $N_\infty$ is the limiting (saturated) concentration of defects after infinitely long exposure to irradiation, and $N_0$ is the initial concentration of these defects. Note that in addition to defect accumulation the above equations describe defect annealing, which formally correspond to the case of $N_0>N_\infty$, reflecting the situation when radiation is decreased or stopped.

When the time is relatively short ($\beta t\ll 1$) the equation for $n$ simplifies to the form

$$n=\frac{G}{\gamma N_0}\frac{1}{\sqrt{1+t/\tau}}, \tag{6}$$

where

$$\tau=\frac{1}{2\beta}\frac{N_0^2}{N_\infty^2-N_0^2},$$

convenient for fitting the experimental results. In the case of considerable degradation the characteristic degradation time $\tau$ is shorter by the factor of $(N_0/N_\infty)^2\ll 1$ than the annealing time $1/\beta$. Therefore Eq. (6) can describe a strong change in concentration ($t/\tau\gg 1$) in the domain of its applicability $\beta t\ll 1$, which is far from saturation. Note that the radiation intensity (proportional to $G$) enters the temporal dependence in Eq. (6) via the product $Gt$, which is the irradiation dose. This means that within the framework of approximation (6) we can consider the $e$ beam either as: (1) being uniformly spread over the scan area (which scales its intensity) during the time of experiment $t_s$ or (2) being concentrated onto local areas of the sample during reduced time $t$ [see Eq. (2)]. Associated with the above alternatives are two characteristic degradation times: (1) the measured degradation time $\tau_s$ corresponding to the first of the above interpretations where the beam is spread uniformly over the time of experiment $t_s$, and (2) the true degradation time $\tau$ under the beam, related to the second of the above interpretations. Note that Eq. (6) predicts the degradation rate $d(\ln n)/dt\propto 1/\tau$ to be approximately linear in the excitation intensity $G$.

A comment is in order regarding other types of recombination centers that may be present in a semiconductor material and not be affected by radiation. They can be formally accounted for by adding a term $-\gamma_1 N_1 n$ in Eq. (4), where $N_1$ is a constant concentration of such centers. This modification makes the solution to Eqs. (3) and (4) rather cumbersome and we do not present it here. We note however that far from saturation [that is in the domain of applicability of Eq. (6)] the annealing process is insignificant, which enables one to write the solution to the modified equations in the form, Eqs. (5) and (6), with $N$ replaced by $N+N_1\gamma_1/\gamma_0$.

Because the parameters $\alpha$, $\beta$, $\gamma$ are temperature dependent, the quantities $N$, $n$, and $\tau$ depend on temperature. As a simple conceivable example we consider a situation when the defects are metastable. Then the annealing barrier is lower than that of defect creation $V_\beta<V_\alpha$. Hence, $N_\infty\propto\exp[(V_\beta-V_\alpha+V_\gamma)/2kT]$ can increase or decrease with temperature depending on the recombination barrier $V_\gamma$. If, on the other hand, the defects are stable, then $V_{\beta>}V_\alpha$ and $N_\infty$ decreases with temperature. Taking into account also that the characteristic time $\tau\propto\gamma\alpha^{-1}\propto\exp[(V_\alpha-V_\gamma)/kT]$ we conclude that the temperature makes degradation either faster or slower depending on the relation between the two barriers.

It should be emphasized that the latter temperature dependence stems from the competition between temperature dependent defect creation and electron recombination rates. In particular, it does not have a bearing upon the annihilation processes represented by the last term in Eq. (3). The physics behind the degradation slowing down in this model is that the nonequilibrium electron concentration responsible for defect creation decreases with time as defects accumulate.

### B. Higher order kinetics

We have been implying above that the kinetics are linear in electron concentration. This simplification may fail if the electron concentration is high. We consider the case when the electron concentration is high enough to make both the defect generation and electron recombination rates quadratic in $n$

$$\frac{dN}{dt}=\alpha n^2-\beta N,\quad G-\gamma Nn^2=0. \tag{7}$$

The recombination rate quadratic in $n$ is known to be one of the limiting cases of the Shockley–Read recombination model. As for the microscopic origin of the defect generation rate quadratic in $n$, this may be due either to defect generation caused by $e-h$ recombination (both electron and hole concentrations enter the probability), or defects with negative Hubbard energy that have two localized electrons or holes per center.[11,12]

Equation (7) has the same solution for $N$ as that in Eq. (5), while the charge carrier concentration becomes

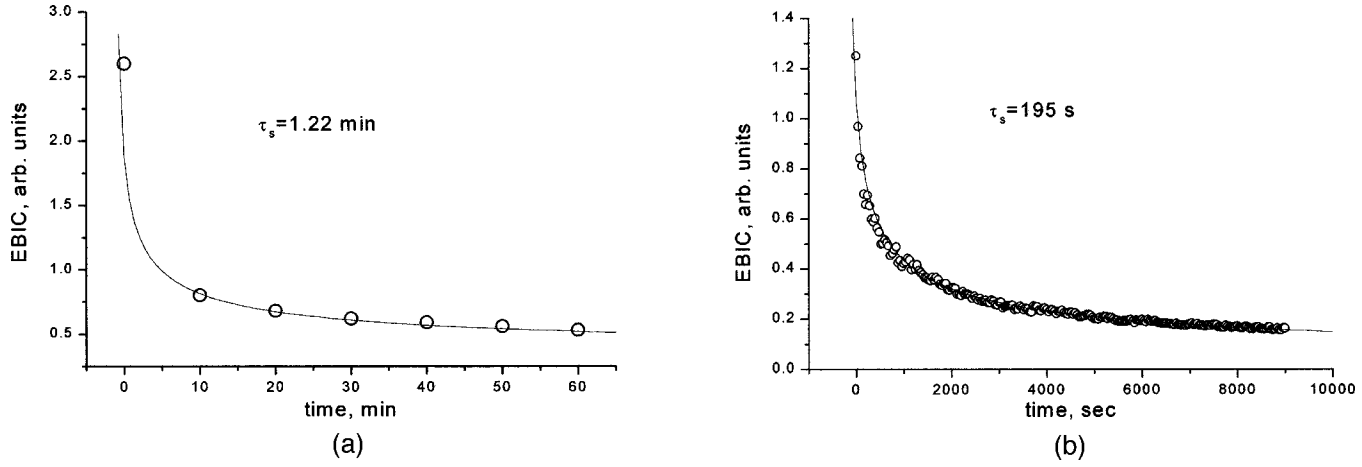


FIG. 7. EBIC degradation data vs theoretical fit by Eq. (6). *e*-beam parameters: (a) $I_e=3.9$ nA, $E=30$ keV, $A=130\ \mu\text{m}^2$; (b) $I_e=0.82$ nA, $E=20$ keV, $A=530\ \mu\text{m}^2$.

$$n=\sqrt{\frac{G}{\gamma N_\infty}}\left\{1-\left[1-\left(\frac{N_0}{N_\infty}\right)^2\right]\exp(-2\beta t)\right\}^{-1/4}$$
$$\rightarrow\sqrt{\frac{G}{\gamma N_0}}\left(1+\frac{t}{\tau}\right)^{-1/4}, \tag{8}$$

where the latter equation is the short time approximation analogous to that in Eq. (6).

In the time domain where annealing is not important (far from saturation) one can describe arbitrary order kinetics

$$\frac{dN}{dt}=\alpha n^\eta, \quad G-\gamma N n^\nu=0, \tag{9}$$

which gives

$$n=\frac{(G/\gamma N_0)^{1/\nu}}{(1+t/\tau)^{1/(\nu+\eta)}}, \quad \tau=\frac{\nu}{\nu+\eta}\left(\frac{\gamma N_0}{G}\right)^{\eta/\nu}\frac{N_0}{\alpha}. \tag{10}$$

The latter result reproduces the approximations in Eqs. (6) and (8). For the case of $\eta=2$ and $\nu=1$ it also reproduces the result[13] devoted to degradations in *a*-Si:H. Note also that Eq. (10) predicts the degradation rate to be nonlinear in the excitation intensity, $d(\ln n)/dt\propto 1/\tau\propto G^{\eta/\nu}$. Substituting the above mentioned parameters $\eta=2$ and $\nu=1$ gives a $G^2$ dependence, in qualitative agreement with $G^{1.8}$ experimentally suggested[14] for the case of *a*-Si:H.

### C. Fitting the experimental data

In fitting the data we assume that the EBIC signal is proportional to the electron concentration $J\propto n$. Most of the data on EBIC degradation versus time can be surprisingly well approximated by the temporal dependence in Eq. (6); some examples are shown in Fig. 7. Fitting various curves gave characteristic true degradation time $\tau$ ranging from 0.3 to 3 s. As seen from Fig. 8, for the case of extremely high energy density, the approximation in Eq. (8) becomes more relevant, and a good fit is achieved for $\tau=0.3$ s.

We also fit the data in Fig. 5 with Eq. (6) where in accordance with Eq. (2) the radiation time was expressed in the terms of scan area. For definiteness we have chosen the end points in each time domain in Fig. 5 and plotted the corresponding area dependence in Fig. 9. Given the variability in EBIC signal between different points, the theory and experiment are in fairly good agreement. The characteristic degradation time determined from this fit was $\tau=1.3$ s.

The data on interrupted degradation in Fig. 4 offer a test for our model prediction that, in accordance with Eq. (6), the absolute value and degradation time of the EBIC signal scales as $(N_0)^{-1}$ and $N_0^2$, respectively. Approximating the two data segments in Fig. 5 by equations $J_1\propto N_{01}^{-1}(1+t/\tau_1)^{-1/2}$, $J_2\propto N_{02}^{-1}[1+(t-70)/\tau_2]^{-1/2}$ gave $\tau_2/\tau_1=4.4$ and $N_{02}/N_{01}=2$, in qualitative agreement with the model prediction.

The nature of the variability in degradation between different spots on the sample (see Fig. 2) requires further discussion. As we have suggested in Sec. II, this variability can be attributed to the local built-in electric fields that make carrier recombination spatially nonuniform. This can be expressed explicitly in our model framework where the main degradation characteristics

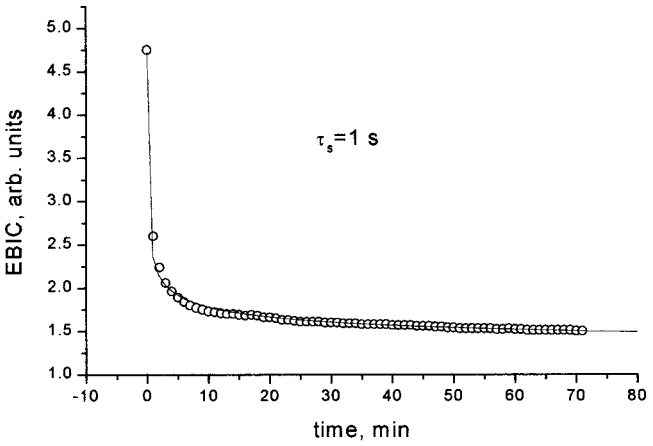


FIG. 8. High intensity EBIC degradation in comparison with the theoretical fit by Eq. (8). *e*-beam parameters: $I_e=1.30$ nA, $E=25$ keV, $A=0.34\ \mu\text{m}^2$.

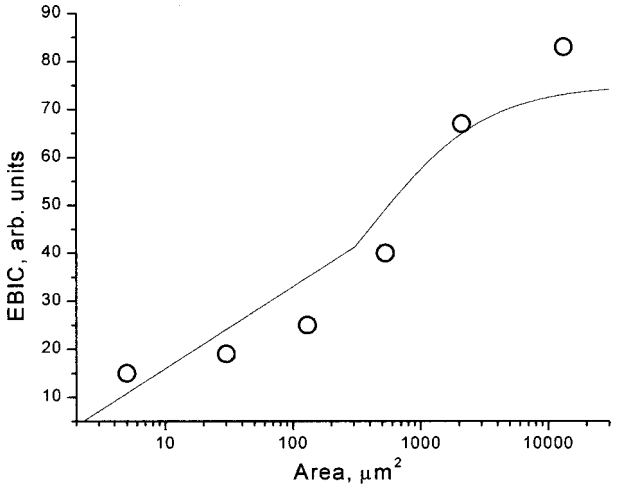


FIG. 9. Area dependence of the EBIC degradation: data vs theoretical fit by $75(1+700/A)^{-1/2}$. The data correspond to the end points of each area time domain in Fig. 5.

$$n(0)=\frac{G}{\gamma N_0}$$

and (11)

$$\tau=\frac{N_0^2\gamma}{G\alpha}$$

depend on the recombination parameter $\gamma\propto\exp(-V_\gamma/kT)$. Available estimates[15] give $V_\gamma\approx 0.8\,\mathrm{eV}$. From this point of view, 100% fluctuation in the degradation kinetics corresponds to 2% fluctuation in $V_\gamma$. The latter is comparable to the relative mean square fluctuation in the interface state concentration $1/\sqrt{sL^2}$, where $s$ is the interface state density ($s\approx 10^{11}-10^{12}\,\mathrm{cm}^{-2}$) and $L$ is the screening length (less than 1 $\mu$m). Hence, strong fluctuations in degradation kinetics can be explained by small statistical fluctuations in the grain boundary parameters. The fact that the observed variability becomes smaller with the dose (Fig. 2) can be attributed to defect accumulation, which decreases the relative concentration fluctuation.

We conclude that the above model gives a fairly good description of the data on *e*-beam degradation. The main feature beyond the scope of our model remains the degree of reversibility of *e*-beam induced degradation.

### D. Other predictions of the model and general discussion

One important question that remains to be addressed is how the observed considerable EBIC degradation relates to the degradation of the electrical characteristics in similar devices illuminated by light. The latter is known to be relatively small for a comparable integral number of generated electron–hole pairs.[16] EBIC degradation corresponds to the decrease in the carrier collection efficiency

$$g=\frac{J}{I_e(W/w)}, \tag{12}$$

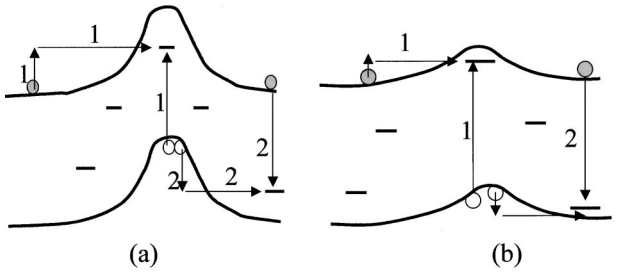


FIG. 10. Electron–hole recombination under the light (a) and EBIC (b) excitations.

which is the ratio between the collected and generated charge carriers. On the other hand, current–voltage measurements reflect the change in device efficiency $\eta$, which is proportional to the open-circuit voltage $V_{oc}$ and short-circuit current $I_{sc}=eN_{ph}qg$ (where $N_{ph}$ is the rate of photon absorption and $q$ is the quantum efficiency).[17] Therefore, both the EBIC signal and the device efficiency are proportional to $g$. The puzzle is that for a comparable integral number of generated electron–hole pairs a relatively big change in EBIC observed in this work is not reflected in the corresponding device efficiency change caused by light radiation.[16]

We suggest an explanation based on the vastly different rates of charge carrier generation in the cases of electron-beam and light irradiation leading to different values of $g$. Indeed, from our EBIC data we estimate $g\sim 0.01$ or less, while $g$ is approximately 1 for good quality devices when illuminated with AM1.5 light. Because $g\cong 1$ means that recombination plays almost no role, it is not surprising that changes in recombination center concentration do not show up in collection efficiency: light-generated carriers are swept away from the device before they can recombine. On the contrary, $g\ll 1$ means that the generated carriers have time to recombine and thus $g$ strongly degrades with accumulation of recombination centers.

We attribute the difference in recombination between the cases of *e*-beam and light to additional screening of the built-in electric fields (both in the main $p-n$ junction and grain boundary regions) by the high-concentration plasma generated by the electron beam. Because of screening, electric fields become less efficient separators of electrons and holes and the latter recombine more readily. For the case of light, the excitation rate is much lower and the screening weaker. Correspondingly, $e-h$ recombination slows down exponentially [$\gamma\propto\exp(-V_\gamma/kT)$] bringing $g$ up to the values close to 1. One can say that the built-in electric fields make the recombination centers less efficient, as is illustrated in Fig. 10. The fact that the *e*-beam generated $e-h$ plasma makes defects more efficient, makes EBIC a ''magnifying glass'' into degradation: radiation induced defects show up stronger in EBIC than in low-intensity light measurements.

One consequence of the above interpretation is the prediction that photoluminescence and cathodoluminescence are suppressed in the vicinity of the grain boundaries. Indeed, because the built-in electric field spatially separates electrons and holes, their radiative recombination slows down as compared to that in the intragrain material where the field is

relatively small or absent. This prediction is consistent with the observations.[10]

Since the recombination properties of the defects become insignificant under the light (and thus the current $I_{sc}$ does not degrade), we consider the change in the other important cell parameter, open circuit voltage $V_{oc}$ due to material compensation. Assuming that $V_{oc}=\text{const}+kT\ln n$, we obtain the degradation time characteristic of $V_{oc}$

$$\tau_V=\left(\frac{dV_{oc}}{V_{oc}dt}\right)^{-1}=\frac{V_{oc}}{kT}\tau\gg\tau. \tag{13}$$

Hence, $V_{oc}$ changes much slower than the defect concentration: the ratio $\tau_\nu/\tau$ is typically in the range of 30–40. Equation (13) describes the difference between the current and $V_{oc}$ degradation under the *e* beam. The $V_{oc}$ degradation under the light will be slower by the ratio of the degradation times under the *e* beam and light.

Summarizing, we can list three factors that make the observed *e* beam and light degradations different: (1) $e-h$ pair generation rate that is much higher for the case of *e* beam; (2) built-in electric fields that are stronger for the case of light; and (3) difference in degrading quantities (current and open circuit voltage for the *e* beam and light, respectively). This understanding is consistent with Eq. (11) for $\tau$ where generation rate is present explicitly, while the built-in electric fields enter via the recombination parameter $\gamma$.

The first of the above factors is quantitatively characterized by the acceleration ratio $a$ [see the discussion after Eq. (1)]. The second factor brings the main uncertainty in translating the observed *e*-beam degradation into that of light. The ratio of the charge carrier lifetimes under light and *e* beam might be a relevant quantitative parameter for this factor. The inverse collection efficiency $g^{-1}$ is its lower bound estimate. The third factor can be estimated by the ratio $\tau_\nu/\tau$ from Eq. (13). In a very rough approximation, we take $a=10^5$, $g^{-1}=100$, $\tau_\nu/\tau=30$ to calculate the translation coefficient of $3\times10^8$ between EBIC and light degradations. With that using typical observed EBIC degradation time $\tau=1$ s gives the lower bound estimate of 10 yr for the light induced degradation time.

One prediction related to our model is that cell degradation rate will be higher under open- then under short-circuit conditions, since in the former case charge carriers accumulate and trigger defect creation. The fact that open-circuit cells degrade faster (but not necessarily stronger) was indeed observed in CdTe-based cells and in $a$-Si based cells.[14,18,19]

Our model predicts metastable defect concentration to increase with temperature even without radiation. Indeed, substituting into Eq. (6) the thermal generation rate $G_T=G_\infty\exp(-E_F/kT)$ gives

$$N_\infty\propto\exp\left(\frac{V_\beta+V_\gamma-V_\alpha-E_F}{2kT}\right),\quad \tau\propto\exp\left(\frac{V_\alpha+E_F-V_\gamma}{kT}\right), \tag{14}$$

where $E_F$ is the Fermi energy. Note that the corresponding degradation time can either increase or decrease with $T$, depending on the recombination barrier height. In particular, annealing of light irradiated samples will not always result in a decrease of the defect concentration; this only happens if the equilibrium dark concentration $N_\infty$ is lower than that under illumination. A related effect predicted by our model is aging of freshly doped samples in the dark. This is described by Eq. (5) when we substitute $G=G_T$ and $N_0=0$

$$n=\sqrt{\frac{G_T\beta}{\gamma\alpha}}\frac{1}{\sqrt{1-\exp(-2\beta t)}}. \tag{15}$$

A comment is in order regarding the temperature dependencies in Eq. (14) and related dependencies mentioned in Sec. III A. The activation barriers $V_\beta$, $V_\gamma$, etc. in those dependencies can be well defined for the case of defects in crystalline structure. In amorphous materials, such as $a$-Si, these barriers are random quantities characterized by their probability distributions. One known consequence of it is that amorphous materials have exponentially wide relaxation time distributions. The longer the stressing time, the slower local configurations are activated by the stress. These low configurations retain their stress-induced changes for a long time after the stress is removed. Therefore, degradation in amorphous structures can be made less recoverable by increasing stress time. For the case of polycrystalline materials this phenomenon could take place in the hypothetical amorphous regions at and between the grain boundaries. We conclude this section by noting that our model predicts cell stability to improve with an increase in the initial concentration of defects $N_0$ and/or the recombination parameter $\gamma$. A consequence of this is that stability can be affected by modifying grain boundaries. It is important that increasing the initial recombination rate does not necessarily result in poorer devices: cell efficiency remains practically intact if the carrier transit time is shorter than the recombination time.

## IV. CONCLUSION

We showed that *e*-beam induced degradation of the CdTe based PV cell can be conveniently measured *in situ* using the EBIC technique. The EBIC signal shows a considerable, continuous degradation depending on the electron-beam current, scan area, and energy. The degradation kinetics is found to fluctuate between different spots on the same sample.

EBIC imaging shows that the grain boundary regions are the most effective carrier collectors. We relate this enhanced collection to the built-in electric fields that effectively separate electrons and holes at the grain boundary regions.

We presented a simple phenomenological model that describes the EBIC degradation as a function of time, scan area, and energy. The model is based on the concept of defects that appear in the system in response to extra electrons and holes generated by radiation and that serve as recombination and compensation centers.

## ACKNOWLEDGMENTS

The authors are grateful to E. Bykov, J. Hanak, U. Jayamaha, V. Kaydanov, G. Nelson, and D. Rose for valuable discussions. This work was supported in part by NREL Thin-Film Partnership Contract No. ZAK-817619-17.

[1] R. H. Bube, *Photovoltaic Materials* (Imperial College Press, London, 1998).
[2] D. Redfield and R. Bube, *Photoinduced Defects in Semiconductors* (Cambridge University Press, Cambridge, 1996).
[3] Libbey-Owens-Ford Co., 1701 E. Broadway St., Toledo, OH 43605.
[4] P. V. Meyers, C. H. Liu, and T. J. Frey, U.S. Patent No. 4,710,589 (1987).
[5] R. Birkmire, 26th IEEE Photovoltaics Conference Proceedings (Anaheim, CA, 1997), p. 295.
[6] D. Grecu and A. D. Compaan, Appl. Phys. Lett. **75**, 361 (1999).
[7] H. C. Chou, A. Rohatgi, N. M. Jokerst, E. W. Thomas, and S. Kamra, J. Electron. Mater. **25**, 7 (1996).
[8] A. L. Fahrenbruch and R. H. Bube, *Fundamentals of Solar Cells* (Academic, New York, 1983); H. J. Leany, L. C. Kimerling, and S. D. Ferris, Scanning Microsc. **1**, 717 (1978).
[9] T. J. McMahon and B. von Roederen, 26th IEEE Photovoltaics Conference Proceedings (Anaheim, CA, 1997), p. 375.
[10] S. A. Galloway, R. P. Edwards, and K. Durose, Inst. Phys. Conf. Ser. **157**, 579 (1997)
[11] D. J. Chadi, Phys. Rev. B **59**, 1581 (1999); F. J. Espinosa, J. M. de Leon, S. D. Conradson, J. L. Pena, and Zapata-Torres, Phys. Rev. Lett. **83**, 3446 (1999).
[12] U. V. Desnica, Vacuum **50**, 463 (1998).
[13] M. Stutzmann, W. Jackson, and C. Tsai, Phys. Rev. B **32**, 23 (1985).
[14] L Yang, L. Chen, J. Y. Hou, and Y. M. Li, Mater. Res. Soc. Symp. Proc. **258**, 365 (1992).
[15] L. M. Woods, D. H. Levi, V. Kaydanov, G. Y. Robinson, and R. K. Ahrenkiel, Proceedings of the 2nd World Conference on Photovoltaic Solar Energy Conversion, Vienna, Austria, July 1998, pp. 1043–1046; V. Kaydanov (private communication).
[16] J. F. Hiltner and J. R. Sites, AIP Conf. Proc. **462**, 170 (1998).
[17] S. M. Sze, *Physics of Semiconductor Devices* (Wiley, New York, 1981).
[18] R. R. Arya, L. Yang, M. Bennett, J. Newton, Y. M. Li, B. Fieselmann, L. F. Chen, K. Rajan, G. Wood, C. Poplawski, and A. Wilczynski, 23th IEEE Photovoltaics Conference Proceedings (Louisville, 1993), p. 790.
[19] R. C. Powell, R. Sasala, G. Rich, M. Steele, K. Bihn, N. Reiter, S. Cox, and G. Dorer, 25th IEEE Photovoltaic Specialists Conference, 1996, p. 785; I. Zulim and I. Vuknic, 14th European Photovoltaic Solar Energy Conference, Barcelona (Washington, 1996), p. 215.